Etrinabdione (VCE-004.8), a B55α activator, promotes angiogenesis and arteriogenesis in critical limb ischemia.

Adela García-Martín, PhD[1,2,3], María E. Prados, PhD[1,2,3], Isabel Lastres-Cubillo [1,3], Francisco J. Ponce-Diaz[1,2,3], Laura Cerero[1,2,3], Martin Garrido-Rodríguez, PhD[4], Carmen Navarrete, PhD[1,3], Rafael Pineda, PhD [1,2,3], Ana B. Rodríguez [1,2,3], Ignacio Muñoz, MD, PhD[1,3], Javier Moya[1,3], Antonella Medeot[1,3], José A. Moreno[1,3], Antonio Chacón, MD, PhD[1,3]. José García-Revillo, MD, PhD[1,3] and Eduardo Muñoz, MD, PhD[1,2,3]

[1] Maimonides Biomedical Research Institute of Córdoba (IMIBIC), Córdoba, Spain.
[2] Cellular Biology, Physiology and Immunology Department, University of Córdoba, Spain.
[3] Hospital Universitario Reina Sofía, Córdoba, Spain.
[4] Heidelberg University, Faculty of Medicine, and Heidelberg University Hospital, Institute for Computational Biomedicine, Bioquant, Heidelberg, Germany.

Short title: Etrinabdione and peripheral artery disease

Corresponding author: Eduardo Muñoz. Maimonides Biomedical Research Institute of Córdoba, University of Córdoba, Avda Menéndez Pidal s/n. 14004. Córdoba, Spain. Phone: +34 677 437513. Email: fi1muble@uco.es

ABSTRACT

Background: Vasculogenic therapies explored for the treatment of peripheral artery disease (PAD) have encountered minimal success in clinical trials. Addressing this, B55α, an isoform of protein phosphatase 2A (PP2A), emerges as pivotal in vessel remodeling through activation of hypoxia-inducible factor 1α (HIF-1α). This study delves into the pharmacological profile of VCE-004.8 (Etrinabdione) and evaluates its efficacy in a preclinical model of critical limb ischemia, with a focus on its potential as a PP2A/B55α activator to induce angiogenesis and arteriogenesis.

Methods: Vascular endothelial cells were used for *in vitro* experiments. Aorta ring assay was performed to explore sprouting activity. Matrigel plug-in assay was used to assess the angiogenic potential. Critical limb ischemia (CLI) in mice was induced by double ligation in the femoral arteria. Endothelial vascular and fibrotic biomarkers were studied by immunohistochemistry and qPCR. Arteriogenesis was investigated by microvascular casting and micro-CT. Proteomic analysis in vascular tissues was analyzed by LC-MS/MS. *Ex-vivo* expression of B55α and biomarkers were investigated in artery samples from PAD patients.

Results: VCE-004.8 exhibited the ability to induce B55α expression and activate the intersecting pathways B55α/AMPK/Sirtuin 1/eNOS and B55α/PHD2/HIF-1α. VCE-004.8 prevented OxLDL and H_2O_2-induced cytotoxicity, senescence, and inflammation in endothelial cells. Oral VCE-004.8 increased aorta sprouting *in vitro* and angiogenesis *in vivo*. In CLI mice VCE-004.8 improved collateral vessel formation and induced endothelial cells proliferation, angiogenic gene expression and prevented fibrosis. The expression of B55α, Caveolin 1 and Sirtuin-1 is reduced in arteries from CLI mice and PAD patient, and the expression of these markers was restored in mice treated with VCE-004.8.

Conclusions: The findings presented in this study indicate that Etrinabdione holds promise in mitigating endothelial cell damage and senescence, while concurrently fostering arteriogenesis and angiogenesis. These observations position Etrinabdione as a compelling candidate for the treatment of PAD, and potentially other cardiovascular disorders.

Keywords: Etrinabdione, VCE-004.8, PPA2/B55α, HIF-1α, Sirtuin 1, eNOS, angiogenesis.

Novelty and Significance

What Is Known?

- The phosphatase PPA2/B55α stabilizes endothelial cells (ECs) in response to cell stress conditions, thereby protecting ECs from apoptosis and promoting angiogenesis.
- Etrinabdione (VCE-004.8) functions as a potent activator of PPA2/B55α inducing PHD2 dephosphorylation at ser125 and fostering HIF activation.
- VCE-004.8 prevents vascular damage in preclinical models of systemic and cardiac fibrosis and alleviates blood-brain barrier disruption in neuroinflammatory conditions.
- VCE-004.8 is also a dual agonist of PPARγ and CB_2 receptors and shows antiinflammatory activity.
- Oral VCE-004.8 has meet the primary endpoints of safety and tolerability in a Phase IIa clinical trial with systemic sclerosis patients (clinicaltrial.gov: NCT03745001).

What New Information Does This Article Contribute?

- Etrinabdione induces HIF-1α expression in endothelial cells through a novel pathway that potentially involves two axes: B55α/PHD2 and B55α/AMPK/Sirt1 signaling that may converge on HIF stabilization.
- Etrinabdione prevented endothelial cell damage and senescence, while inducing arteriogenesis and angiogenesis in CLI mice.
- In arteries of patients with PAD and in CLI mouse models, the expression levels of B55α, Caveolin 1, and Sirtuin 1 are diminished. However, treatment with Etrinabdione specifically in CLI mice prompts an increase in the levels of these proteins.
- Etrinabdione triggers neovascularization and angiogenesis specifically within hypoxic tissue in a critical ischemia model, with no impact on healthy tissue.

93 **INTRODUCTION**

94

95 Peripheral arterial disease (PAD) is one of the major leading cause of atherosclerotic
96 cardiovascular morbidity[1]. Experimental approaches to the treatment of PAD have
97 included the use of angiogenic factors as a recombinant protein or as gene therapy as well
98 as stem cell therapy[2] but, neither of these strategies achieved significant benefits in
99 clinical trials. Hence, there is an urgent demand for novel pharmacological targets and
100 therapies capable of preventing endothelial damage and promoting angiogenesis and
101 arteriogenesis to enhance blood flow in extremities.

102 The protein phosphatase 2A (PP2A) belong to a family of serine-threonine
103 phosphatases, which are formed by a catalytic C subunit, a scaffold A subunit, and a
104 regulatory B subunit, which confers specificity of PP2A for selective proteins substrates[3].
105 B55α (PPP2R2A) is one of the regulatory subunits that has been shown to directly
106 dephosphorylates prolyl hydroxylase 2 (PHD2) on Ser125, resulting in a further reduction
107 of its activity that ultimately stabilized and accumulated the hypoxia inducing factor 1α
108 (HIF-1α)[4]. HIF-1, a heterodimeric basic-helix-loop-helix-paste protein that responds to
109 oxygen tension, is activated by severe and mild hypoxia. Under hypoxic conditions, HIF-
110 1α accumulates in the nucleus and dimerizes with HIF-1β to activate a plethora of genes
111 including angiogenic factors such as vascular endothelial growth factor (VEGF),
112 fibroblast growth factor (FGF) and angiopoietin, as well as an important number of genes
113 involved in vascular and tissue remodeling.[5,6] HIF-1α is also activated by therapeutic
114 preconditioning hypoxia and by hypoxia mimetic small compounds.[7,8] More recently, it
115 has been shown that B55α stabilizes endothelial cells (ECs) in response to cell stress
116 conditions, thereby protecting ECs from apoptosis and promoting angiogenesis. Thus,
117 PP2A/B55α activators represent a new class of hypoxia mimetic compounds with
118 potential in vessel remodeling, angiogenesis and endothelial cell protection[9].

119 The histone deacetylase Sirtuin 1 (Sirt1) belong to the family of Sirtuins, which
120 are nicotinamide adenine dinucleotide (NAD^+)-dependent enzymes with multiple
121 metabolic functions. The expression of Sirt1 is reduced with aging both in animal models
122 and in humans, and a reduced expression is thought to be involved in age-related
123 cardiovascular diseases. Indeed, Sirt1, which is activated by AMPK, is a critical
124 modulator of the vascular function[10] and endothelial senescence is regarded as a
125 prominent precursor of cardiovascular diseases including PAD and critical limb ischemia
126 (CLI).[11] The key role of Sirt1 in the regulation of vascular homeostasis is mediated

through complex cellular mechanisms involved in the promotion of vasodilatory and regenerative functions at ECs, endothelial progenitor cells, and smooth muscle cells (SMC) levels.[12]

We have recently identified the cannabidiol aminoquinone VCE-004.8 (also known as Etrinabdione and EHP-101), as a PP2A/B55α activator that induces HIF-1α and HIF-2α stabilization.[13] In addition, VCE-004.8 is a dual activator of peroxisome proliferator-activated receptor-γ (PPARγ) and cannabinoid type 2 receptors (CB_2R).[14] VCE-004.8 showed efficacy in preclinical models of traumatic brain injury,[15] multiple sclerosis[13], bleomycin- and angiotensin-induced models of dermal, lung, cardiac, and kidney fibrosis[14, 16], metabolic syndrome[17] and stroke[18].

Etrinabdione (VCE-004.8) has finalized the stage 1 of a clinical Phase IIa trial in Systemic Sclerosis patients (Clinical Trials.gov: NCT04166552), and it had acceptable safety profile and was well-tolerated. Herein we have further investigated additional pharmacological attributes of VCE-004.8 and explored its efficacy in a model of CLI.

METHODS

Please see the Supplemental Material for detailed methods on cell cultures, transient transfections and luciferase assays, western blot analysis, measurement of NO (nitric oxide), Sirtuin 1 activity, NAD^+ /NADH ratio, senescence assay, aortic ring assay, *in vivo* angiogenesis, in *vivo* perfusion fixation and tissue processing procedures, confocal immunofluorescence microscopy, qPCR, and proteomic analysis). All experimental protocols followed the guidelines of animal care set by the EU guidelines 86/609/EEC, the Ethic Committee on Animal Experimentation at the University of Córdoba (Spain) and the Andalusian Regional Committee for Animal Experimentation approved all the procedures described in this study (31/03/2022/057). Human biopsies from patients were obtained by the Cardiovascular Surgery Unit of Hospital Universitario Reina Sofia of Cordoba, Spain (RSUH) and the protocol approved from the Ethics Committee of RSUH (reference: HIP-CI:1.0-01/06/2023).

Data Availability. The data that support the findings of this study are available from the corresponding author upon request.

160 **Test compound.** VCE-004.8 (also called Etrinabdione and EHP-101) [(1′R,6′R)−3-
161 (Benzylamine)−6-hydroxy-3′-methyl-4-pentyl-6′-(prop-1-en-2-yl) [1,1′bi(cyclohexane)
162]− 2′,3,6-triene-2,5-dione)] was produced under GMP conditions and provided by
163 VivaCell Biotechnology España, Spain). For animal use VCE-004.8 was dissolved in
164 sesame oil/Maisine CC® (50%/50%) and applied by oral gavage.
165
166 **Critical limb ischemia (CLI) mouse model**. Male C57BL/6 mice aged 10-12 weeks
167 were divided into 2 groups (CLI group and sham group). In the CLI group the femoral
168 artery and its side branches were double ligated with 6–0 silk sutures immediately distal
169 to the inguinal ligament and proximal to the popliteal bifurcation. Femoral nerves were
170 carefully preserved. The wound was irrigated with sterile saline and then the overlying
171 skin was closed using 4–0 vicryl sutures. Post-operative pain was reduced using
172 Lignocaine. A similar surgery without ligation of the femoral artery was performed on
173 the sham controls. The CLI group was administered VCE-004.8 (20 mg/kg) by oral
174 gavage every day until the end of the study and the sham control group was treated with
175 vehicle (Corn oil/Maisine® CC (50/50 (v/v)). At 10 and 28 days after ligation, the whole
176 limb and muscles were harvested for study.
177
178 **Vascular casting.** Mice were anesthetized and injected 1000 UI of heparin (i.p.). After
179 10 min, the mice were euthanized, the thorax was opened, and the aorta exposed. A
180 catheter was inserted into the descending aorta and fixed with sutures. Then mice were
181 perfused with PBS (37 °C, 80 ml) containing heparin, nitroglycerin, adenosine and
182 sodium nitroprusside to remove the blood and enhanced the vasodilatation of the vessels.
183 Microfil (MV-112 [white]; Flow Tech Inc, South Windsor, CT, USA) was perfused and
184 then filled the entire vascular bed. The Microfil polymerized overnight at 4°C, and the
185 samples were harvested and clarified in graded glycerol solutions (40%–100% glycerol
186 in water; glycerol increased by 20% at 24-hour intervals). The clarified specimens were
187 viewed on a dissecting microscope and Microfil retained in the vasculature was
188 investigated by μ-CT (X-ray tomography).
189
190 **Image acquisition μ-CT.** After Microfilm polymerization, the animals were hold inside
191 a Bruker SkyScan 1172 high resolution microtomography machine (Bruker micro-CT,
192 Kontich, Belgium). The X-ray source was set to a voltage of 50 kV and a current of 498
193 μA with a 0.5-mm Al filter in the beam path with an angular increment of 0.3°. Data were

194 transferred to a computer with NRecon, CTAn, CT Vol software, (Bruker), ImageJ
195 (http://rsb.info.nih.gov/ij/) and 3DSlicer v.3.4.0 open-source software
196 (https://pubmed.ncbi.nlm.nih.gov/22770690/) was using to analyze vessel numbers,
197 diameter, area, and volume, as well as arterial density.
198
199 **Laser capture microdissection (LCM) targeted mass spectroscopy.** LCM and
200 subsequent molecular analysis were carried out on slides immuno-stained using anti-α-
201 Smooth Muscle Actin (α-SMA) antibody of gastrocnemius muscles frozen sections. The
202 vessel marked with immunofluorescence α-SMA were dissected with ZEISS PALM
203 Microbeam micro dissected and collected for mass spectroscopy analysis.
204
205 **Proteomics data analysis.** To generate Figure 7B, we employed the log transformed
206 intensities for proteins annotated with the Gene Ontology term 'Angiogenesis' (GO:
207 0001525). The mass spectrometry proteomics data have been deposited to the
208 ProteomeXchange Consortium via the PRIDE partner repository with the dataset
209 identifier PXD050360.
210
211 **Statistical Analysis.** Data were expressed as the mean ± SEM or SD. One-way analysis
212 of variance (ANOVA) followed by the Tukey´s post-hoc test for parametric analysis or
213 Kruskal-Wallis post-hoc test in the case of non-parametric analysis tests will be used to
214 determine the statistical significance. The level of significance will be set at $p< 0.05$.
215 Statistical analyses will be performed using GraphPad Prism version 9 (GraphPad, San
216 Diego, CA, USA).
217
218 **RESULTS**
219
220 **VCE-004.8 induces B55α/PP2A in endothelial vascular cells.** We have demonstrated
221 that VCE-004.8, a hypoxia-mimetic cannabidiol aminoquinone derivative,
222 dephosphorylates PHD2 at ser-125 via a PP2A/B55α-dependent pathway, leading to the
223 induction of HIF-1α expression[13]. In this study, we further reveal that B55α expression in
224 EA-hy926 cells is primarily localized perinuclearly and is significantly upregulated
225 following exposure to VCE-004.8 (Fig. 1A). As anticipated, silencing B55α expression
226 with siRNA in EA-hy926 cells abrogated the VCE-004.8-induced stabilization of HIF-1α
227 (Fig. 1B). To investigate the functional impact of VCE-004.8 and HIF-1α on cell viability,

228 we subjected the cells to H_2O_2 treatment in the presence or absence of the compound.
229 VCE-004.8 greatly prevented H_2O_2-cytotoxicity in a concentration-dependent manner
230 (Fig. 1C), which was significantly counteracted by YC-1, a HIF-1α inhibitor (Fig. 1D).
231 Moreover, the cytoprotective effect of VCE-004.8 was evident in cells exposed to both
232 high glucose and OxLDL (Fig. 1S). Subsequently, to explore the anti-inflammatory
233 properties of VCE-004.8, EA-hy926 cells were incubated with proinflammatory
234 cytokines, and the expression of various markers was analyzed via confocal microscopy.
235 VCE-004.8 attenuated IL-1β+TNFα-induced VCAM-1 expression and restored the
236 expression of tight-junction proteins ZO-1 and CLD1 in IL-6/TNFα-treated cells.
237 Notably, tight-junction proteins play a crucial role in maintaining the integrity of vascular
238 endothelial cells[19]. Furthermore, VCE-004.8 also induced the expression of B55α under
239 inflammatory conditions (Fig. 2S).
240
241 **VCE-004.8 activates AMPK/Sirtuin-1 and prevents senescence in endothelial**
242 **vascular cells.** The protective role of the AMP-activated Protein Kinase (AMPK)
243 pathway, a pivotal cellular energy sensor, extends beyond metabolic homeostasis to
244 encompass cardiovascular protection. Vascular AMPK plays a crucial role in regulating
245 endothelial function, redox homeostasis, and inflammation.[20] Moreover, emerging
246 evidence indicates a functional interplay between AMPK and HIF pathways, contributing
247 to cellular survival adaptation[21]. Thus, we interrogated the participation of AMPK on the
248 pathways activated by VCE-004.8 in endothelial cells. VCE-004.8 induced AMPK
249 phosphorylation and upregulated the expression of Sirt1 and nicotinamide
250 phosphoribosyl transferase (NAMPT), also known as Visfatin, in EA.hy926 cells (Fig.
251 2A and 2B). A connection between AMPK and Sirt1 has been proposed since AMPK
252 activates Sirt1 through an increase in cellular NAD^+ level [22], while Sirt1 deacetylates the
253 AMPK kinase LKB1, leading to phosphorylation and activation of AMPK[23]. We found
254 that VCE-004.8 increases the enzymatic activity of Sirt1 and the NAD^+/NADPH ratio in
255 EA-hy926 cells (Fig. 2C and D). Moreover, silencing Sirt1 expression with siRNA
256 prevented the induction of HIF-1α expression by VCE-004.8 (Fig. S3A). To further
257 explore the effect of VCE-004.8 on cellular senescence EA.hy926 cells were treated with
258 H_2O_2 and the expression of both SA-β-gal^+ cells, Sirt1 and p21 proteins analyzed. VCE-
259 004.8 significantly inhibited H_2O_2-induced senescence and p21 expression and restored
260 the expression of Sirt1 that was downregulated with the H_2O_2 treatment (Fig. 2E and 2F).
261 In addition, pretreatment with dorsomorphin (DS), an AMPK inhibitor, or EX527, a Sirt1

262 inhibitor, separately or in combination, also inhibited both VCE-004.8-induced EPO-Luc,
263 serving as a surrogated marker of HIF activation (Fig. S3B), and H_2O_2-induced
264 cytotoxicity (Fig. S3C). We also investigated eNOS phosphorylation at ser1177, another
265 target of AMPK, and observed that VCE-004.8 induced eNOS phosphorylation (Fig. 3A)
266 as well as NO production (Fig. 3B) in EA.hy926 cells. Interestingly, eNOS
267 phosphorylation was significantly diminished in B55α siRNA cells, providing further
268 evidence for the functional interaction between B55α and AMPK in response to VCE-
269 004.8. Taken together, these findings suggest that in addition to PHD2/HIF-1α activation,
270 the AMPK/Sirt1/eNOS signaling pathways play a significant role in the mechanism of
271 action of VCE-004.8.
272
273 **Angiogenic and arteriogenic effects of VCE-004.8.** Vascular regeneration,
274 angiogenesis, arteriogenesis and vasculogenesis are the main objectives for potential
275 vasculogenic therapies for PAD[24]. To evaluate the effect of VCE-004.8 in vascularization
276 and sprouting, we performed an *ex vivo* aortic ring assay. We found that VCE-004.8, as
277 well as VEGF and dimethyloxallyl glycine (DMOG), an enzymatic Pan-PHD inhibitor,
278 induced vascularization *in vitro*, indicated by the formation of new sprouts as well as
279 sprout area (Fig. S4A). Next, to investigate the angiogenic potential of VCE-004.8 in
280 vivo, we conducted a Matrigel plug *in situ* assay. After ten days following the
281 subcutaneous injection of Matrigel into the flank, no signs of angiogenesis were observed
282 in the negative control group (without treatment), in contrast to Matrigel embedded with
283 VEGF (positive control). Oral treatment with VCE-004.8 (10 and 20 mg/kg) clearly
284 increased the formation of functional vessel identified by $CD31^+/\alpha SMA^+$ staining and the
285 proliferative activity of vascular endothelial cells were identified by expression of
286 $CD31^+/Ki67^+$ cells. Moreover, we also confirmed that B55α is also expressed in the new
287 formed vessels (Fig. S4B).
288 To further explore the effect of VCE-004.8 in a model of critical limb ischemia
289 (CLI) a doble ligation in the femoral arteria was performed in mice and 24 h later animals
290 were treated daily with oral VCE-004.8. After 10 or 28 days of treatment the effect of
291 VCE-004.8 on collateral vessels was investigated by vascular casting and microcomputed
292 tomography (μ-CT) imaging. It is shown in Figure 4A that treatment with VCE-004.8
293 clearly induced collateral artery formation in the ligated limb compared to the non-ligated
294 control limb, which was not affected by the treatment. These results are in good

295 correlation with the mRNA expression of *Hif1α* and the HIF-regulated proangiogenic
296 genes *Vegfa*, *Epo* and *Hgf* in the gastrocnemius muscle in the affected limb but not in
297 control limb (Fig. 4B) suggesting that the effect of VCE-004.8 is specific to damaged
298 tissues.
299
300 **Angiogenic and antifibrotic effects of VCE-004.8 in CLI mice.** Reperfusion of
301 ischemic tissues depends on angiogenesis that is required for a proper tissue blood flow[25,
302 26]. Thus, we explored the effect of VCE-004.8 on angiogenesis and vascular density in
303 the gastrocnemius tissue. VCE-004.8 induced angiogenesis measured by the number of
304 vessels ($CD31^+/\alpha SMA^+$) and lumen perimeter vessel per area in the ligated limb without
305 affecting the contralateral limb (Fig. 5A). We also investigated endothelial cells
306 proliferation, a key event in angiogenesis, and found that VCE-004.8 significantly
307 induced cell proliferation as measured by CD31/Ki67 co-staining (Fig. 5B). CD34 is one
308 of the surface markers for endothelial progenitor cells, which plays a major role in
309 angiogenic and vasculogenic activities during neovascularization[27]. Indeed, $CD34^+$ cells
310 isolated from peripheral blood have been widely used in experimental therapies including
311 cardiovascular diseases and critical leg ischemia[28, 29]. VCE-004.8 treatment significantly
312 increased the average the of number of $CD34^+/CD31^+$ as well as $CD34^+/CD31^-$ cells in
313 the ligated limb compared with the contralateral limb (Fig. 6A).
314 Evidence supports the involvement of fibrosis in the pathophysiology of PAD[30].
315 Fibrosis is associated with various pathological processes in vascular tissues and may
316 contribute to the progression of PAD[31]. Herein, we investigated the expression of
317 Tenascin C (TNC), a marker for fibrosis in both CLI mice and in ex-vivo human samples
318 from PAD patients [32]. TNC expression was detected in the ligated limb of CLI mice (Fig.
319 6B) and human aorta from PAD patients (Fig. 6C) and treatment with VCE-004.8
320 significantly alleviated TNC deposition in the ischemic tissue relative to the contralateral
321 leg (Fig. 6B).
322
323 **B55α and Sirtuin 1 expression in CLI mice and human arteries.** As demonstrated
324 above, our data revealed a mechanistic link between B55α and Sirt1 expression and
325 activity in vitro. Consequently, we investigated the expression of both proteins in tissues.
326 B55α and Sirt1 expression were found to be downregulated in the ligated limb from CLI
327 mice compared to the contralateral limb (Fig. 7A and 7B), and similar results were

328 observed in the aorta from PAD patients (diseased) compared to healthy tissues (Fig. 7D).
329 VCE-004.8 treatment completely restored the expression of both proteins in the ligated
330 limb of CLI mice. The mRNA expression levels of B55α and Sirt1 confirmed the findings
331 obtained from confocal analysis. Additionally, VCE-004.8 exhibited a tendency to
332 increase the mRNA expression of Sirt1 in the non-ligated limb of CLI mice (Fig. 7C).
333
334 **Caveolin 1 is downregulated in CLI mice and human arteries.** To investigate the
335 effects of VCE-004.8 on the expression of other markers, we labeled the tissues with
336 αSMA to identify mature vessels. These vessels were subsequently isolated and studied
337 using Laser Capture Microdissection coupled to Mass Spectrometry (Fig. 8A). From the
338 total bulk of proteins (210), eleven proteins involved in the angiogenesis process were
339 identified according to Gene Ontology Annotations from Mice Genomic Identification [33].
340 Among them, caveolin 1 (CAV1) is of special interest in our study since its gene is
341 regulated by HIF-1[34] and it is required for collateral development in CLI mice [35] (Fig.
342 8B). The expression of CAV1 was detected in both the control limb of CLI mice and in
343 healthy human arteries (Fig. 8C and 8E), while it was downregulated in the ligated limb
344 of CLI mice and in arteries affected by PAD (Fig. 8C and 8E). Treatment with VCE-
345 004.8 normalized the expression of CAV1 protein and upregulated its mRNA expression
346 (Fig. 8C and 8D).
347
348 **DISCUSSION**
349
350 Effective induction and promotion of angiogenesis have been so far very challenging. A
351 better knowledge of the basic pro-angiogenic players will be crucial to achieve a clinical
352 benefit for PAD patients and other cardiovascular diseases. Therapeutic angiogenesis or
353 vascular regeneration remains an attractive treatment modality for PAD and chronic
354 tissue ischemia. Despite decades of research into angiogenic and cell-based therapies for
355 PAD, their translation to clinical use has been limited. Therefore, there is an urgent need
356 for novel therapeutic angiogenic approaches.
357 Vascular regeneration strategies include restoration of vascular function and
358 structure that can be partially achieved through HIF activation. While severe hypoxia can
359 be detrimental, leading to cell death and organ failure, mild hypoxia, also known as
360 hypoxia preconditioning, has shown promising therapeutic potential, particularly in the
361 treatment of cardiovascular diseases[36]. Mild hypoxia can be achieved by hypoxia mimetic

362 enzymatic inhibitors of PHDs such are JNJ-42041935, FG-4497, FG-4592 (Roxadustat),
363 TRC160334 (Desidustat), and AKB-4924 [37] or by novel PPA2/B55α activators such are
364 Etrinabdione (VCE-004.8) and VCE-005.1[13,38]. Indeed, it has been observed that the
365 enzymatic inhibitor of PHDs, FG-4497, confers protection against the development of
366 atherosclerosis, a pivotal factor in PAD pathogenesis [39]. Herein, we show the sprouting
367 and angiogenic activity of VCE-004.8 *in vitro* and *in vivo* and its efficacy in CLI mice
368 induced by femoral ligation. Etrinabdione induced endothelial cells proliferation,
369 angiogenic gene expression and prevented fibrosis. One striking and interesting
370 observation is that the effects of Etrinabdione occur only in the affected limbs compared
371 to non-ischemic limbs. A similar observation was found with sodium nitrite therapy and
372 metformin in CLI mice [40, 41] and these results agree with our previous finding showing
373 that VCE-004.8 induced angiogenesis and restored damaged brain blood barrier in the
374 affected brain hemisphere of mice with traumatic brain injury but in the contralateral
375 hemisphere [13]. Thus, we could speculate that the therapeutic benefit of Etrinabdione will
376 be akin to converting severe hypoxia into therapeutic mild hypoxia in the affected limb.
377 The pathophysiology of atherothrombosis and PAD is complex, and involves
378 many cells, proteins and pathways, giving the possibility to explore multitarget
379 therapeutic strategies, which by covering different angles of the disease may be beneficial
380 for the outcome of patients. Herein we show that Etrinabdione, a multitarget drug
381 candidate in clinical phases, induces HIF-1α expression in endothelial cells through a
382 novel pathway that potentially involves two axes: B55α/PHD2 and B55α/AMPK/Sirt1
383 signaling that may converge on HIF stabilization. In addition, VCE-004.8 induces the
384 phosphorylation of eNOS at ser1177, which is a target for AMPK. How B55α regulates
385 AMPK needs to be investigated at the molecular level but previous studies have revealed
386 that AMPK signaling regulates the nuclear accumulation of HIF-1α through a complex
387 process involving HDAC5 phosphorylation. This process leads to the export of HDAC5
388 from the nuclei to the cytosol, where it dissociates the complex formed by the HSP70
389 chaperone and nascent HIF-1α [42]. Subsequently, HIF-1α associates with HSP90,
390 facilitating its maturation and relocation into the nucleus. Notably, treatment with
391 CCT018159, an HSP90 inhibitor, partially inhibits VCE-004.8-induced HIF-1α
392 stabilization (Fig. S5). Moreover, Sirt1 interacts with AMPK and HIF-1α, and
393 pharmacological inhibition of Sirt1 impairs HIF-1α nuclear accumulation and the
394 expression of HIF-1α-dependent genes [43]. Therefore, it is probable that VCE-004.8

395 requires AMPK to enhance the synthesis of nascent HIF-1α, and B55α/PHD2 to stabilize
396 and translocate this nuclear factor into nuclei. This is supported by our results showing
397 that metformin, an AMPK activator that phosphorylates eNOS [39] but did not activate HIF-
398 1α in vascular endothelial cells[44]. However, it is noteworthy that metformin has been
399 shown to promote revascularization in CLI mice independently of HIF-1α [41].

400 In addition, VCE-004.8 is a dual agonist of PPARγ and CB_2R[14]. PPARγ and CB_2R
401 are preclinically validated therapeutic targets for vascular inflammation and
402 atherosclerosis [45,46,47]. For instance, foam cells play a vital role in the initiation and
403 development of atherosclerosis since they are the major sources of necrotic core in
404 atherosclerotic plaques. Interestingly, it has been shown that PPARγ agonists inhibit the
405 formation of macrophage foam cells *in vivo*[48]. Moreover, JHW-015, a CB_2R agonist,
406 significantly prevented oxLDL accumulation in foam cells and reduced the production of
407 proinflammatory cytokines and the expression of CD36, a scavenger receptor that plays
408 a critical role in the formation of foam cells. In agreement with finding CB_2R activation
409 by WIN55,212-2 also reduces an OxLDL-induced inflammatory response in rat
410 macrophages[49]. In line with this we have found that VCE-004.8 inhibits the induction of
411 foam cells in OxLDL-treated macrophages (Fig. S6).

412 On the other hand, VCE-004.8 has also shown efficacy in a murine model of
413 metabolic syndrome induced by high-fat diet. VCE-004.8 showed anti-obesity and anti-
414 inflammatory activity, prevented liver damage and significantly improved glycolipid
415 metabolism[17]. If this activity had translation in humans, we could expect an added benefit
416 in PAD patients with type II diabetes as co-morbidity. The same hold true for coexisting
417 cerebrovascular or coronary diseases since VCE-004.8 showed efficacy in a preclinical
418 stroke model with an excellent therapeutic window and inhibited angiotensin-II signaling
419 and cardiac inflammation and fibrosis[16,18].

420 In many cases, diseases with complex physiopathology are very difficult to be
421 treated by monotargeted therapies, and usually requires concomitant therapies
422 (polypharmacy) that have limitations such as therapy adherence and pharmacological
423 interactions. In contrast, multipronged therapies (polypharmacology) may represent
424 potential pharmacological therapies with better clinical benefits after providing a safe
425 profile in humans and an appropriated target engagement as it is the case of reprofiling
426 therapies with small molecules[50].

427

CONCLUSIONS

In conclusion, our results collectively demonstrate that VCE-004.8 is a first-in-class activator of PP2A/B55α, a phosphatase critical for vascular endothelial cell homeostasis through HIF-1 stabilization and activation. Furthermore, VCE-004.8 activates the AMPK/Sirt1/eNOS pathway in a PP2A/B55α-dependent manner, showing potential in preventing endothelial cell damage and senescence, while also promoting arteriogenesis and angiogenesis in CLI mice. Moreover, the supplementary anti-inflammatory properties of Etrinabdione position it as a potential disease-modifying drug, offering clinical benefits to PAD patients with diverse comorbidities

ACKNOWLEDGMENTS

We acknowledge the Microscopy Advanced Optical Microscopy and the Proteomic Units of IMIBIC for its support.

SOURCES OF FUNDING

This work was supported by grants PID2020-114753RB-I00 (Agencia Estatal de Investigación, Spain; co-funded with EU funds from FEDER Program) and CPP2021-008557/AEI/10.13039/501100011033/Unión Europea NextGenerationEU/PRTR.

DISCLOSURES

AGM, ILC, and EM have applied for a European Patent based on some of the data presented herein.

450 **REFERENCES**

451

452 1. Annex BH, Cooke JP. New Directions in Therapeutic Angiogenesis and
453 Arteriogenesis in Peripheral Arterial Disease. *Circ Res*. 2021;128:1944–1957.
454 2. Beckman JA, Schneider PA, Conte MS. Advances in Revascularization for
455 Peripheral Artery Disease: Revascularization in PAD. *Circ Res*. 2021;128:1885–
456 1912.
457 3. Clark AR, Ohlmeyer M. Protein phosphatase 2A as a therapeutic target in
458 inflammation and neurodegeneration. *Pharmacology & Therapeutics*.
459 2019;201:181–201.
460 4. Di Conza G, Trusso Cafarello S, Loroch S, Mennerich D, Deschoemaeker S, Di
461 Matteo M, Ehling M, Gevaert K, Prenen H, Zahedi RP, et al. The mTOR and PP2A
462 Pathways Regulate PHD2 Phosphorylation to Fine-Tune HIF1α Levels and
463 Colorectal Cancer Cell Survival under Hypoxia. *Cell Reports*. 2017;18:1699–1712.
464 5. Appelhoff RJ, Tian Y-M, Raval RR, Turley H, Harris AL, Pugh CW, Ratcliffe PJ,
465 Gleadle JM. Differential Function of the Prolyl Hydroxylases PHD1, PHD2, and
466 PHD3 in the Regulation of Hypoxia-inducible Factor. *Journal of Biological*
467 *Chemistry*. 2004;279:38458–38465.
468 6. Watts ER, Walmsley SR. Inflammation and Hypoxia: HIF and PHD Isoform
469 Selectivity. *Trends in Molecular Medicine*. 2019;25:33–46.
470 7. Olenchock BA, Moslehi J, Baik AH, Davidson SM, Williams J, Gibson WJ,
471 Chakraborty AA, Pierce KA, Miller CM, Hanse EA, et al. EGLN1 Inhibition and
472 Rerouting of α-Ketoglutarate Suffice for Remote Ischemic Protection. *Cell*.
473 2016;164:884–895.
474 8. Liang Y, Ruan W, Jiang Y, Smalling R, Yuan X, Eltzschig HK. Interplay of hypoxia-
475 inducible factors and oxygen therapy in cardiovascular medicine. *Nat Rev Cardiol*.
476 2023;20:723–737.
477 9. Ehling M, Celus W, Martín-Pérez R, Alba-Rovira R, Willox S, Ponti D, Cid MC,
478 Jones EAV, Di Conza G, Mazzone M. B55α/PP2A Limits Endothelial Cell
479 Apoptosis During Vascular Remodeling: A Complementary Approach To Disrupt
480 Pathological Vessels? *Circ Res*. 2020;127:707–723.
481 10. Ministrini S, Puspitasari YM, Beer G, Liberale L, Montecucco F, Camici GG. Sirtuin
482 1 in Endothelial Dysfunction and Cardiovascular Aging. *Front. Physiol.*
483 2021;12:733696.
484 11. Han Y, Kim SY. Endothelial senescence in vascular diseases: current understanding
485 and future opportunities in senotherapeutics. *Exp Mol Med*. 2023;55:1–12.
486 12. D'Onofrio N, Vitiello M, Casale R, Servillo L, Giovane A, Balestrieri ML. Sirtuins
487 in vascular diseases: Emerging roles and therapeutic potential. *Biochimica et*
488 *Biophysica Acta (BBA) - Molecular Basis of Disease*. 2015;1852:1311–1322.
489 13. Navarrete C, Carrillo-Salinas F, Palomares B, Mecha M, Jiménez-Jiménez C, Mestre
490 L, Feliú A, Bellido ML, Fiebich BL, Appendino G, et al. Hypoxia mimetic activity
491 of VCE-004.8, a cannabidiol quinone derivative: implications for multiple sclerosis
492 therapy. *J Neuroinflammation*. 2018;15:64
493 14. Del Río C, Navarrete C, Collado JA, Bellido ML, Gómez-Cañas M, Pazos MR,
494 Fernández-Ruiz J, Pollastro F, Appendino G, Calzado MA, et al. The cannabinoid
495 quinol VCE-004.8 alleviates bleomycin-induced scleroderma and exerts potent
496 antifibrotic effects through peroxisome proliferator-activated receptor-γ and CB2
497 pathways. *Sci Rep*. 2016;6:21703.
498 15. Navarrete C, García-Martín A, Correa-Sáez A, Prados ME, Fernández F, Pineda R,

Mazzone M, Álvarez-Benito M, Calzado MA, Muñoz E. A cannabidiol aminoquinone derivative activates the PP2A/B55α/HIF pathway and shows protective effects in a murine model of traumatic brain injury. *J Neuroinflammation*. 2022;19:177.

16. García-Martín A, Navarrete C, Garrido-Rodríguez M, Prados ME, Caprioglio D, Appendino G, Muñoz E. EHP-101 alleviates angiotensin II-induced fibrosis and inflammation in mice. *Biomedicine & Pharmacotherapy*. 2021;142:112007.
17. Palomares B, Ruiz-Pino F, Navarrete C, Velasco I, Sánchez-Garrido MA, Jimenez-Jimenez C, Pavicic C, Vazquez MJ, Appendino G, Bellido ML, et al. VCE-004.8, A Multitarget Cannabinoquinone, Attenuates Adipogenesis and Prevents Diet-Induced Obesity. *Sci Rep*. 2018;8:16092.
18. Lavayen BP, Yang C, Larochelle J, Liu L, Tishko RJ, De Oliveira ACP, Muñoz E, Candelario-Jalil E. Neuroprotection by the cannabidiol aminoquinone VCE-004.8 in experimental ischemic stroke in mice. *Neurochemistry International*. 2023;165:105508.
19. Claesson-Welsh L, Dejana E, McDonald DM. Permeability of the Endothelial Barrier: Identifying and Reconciling Controversies. *Trends in Molecular Medicine*. 2021;27:314–331.
20. Rodríguez C, Muñoz M, Contreras C, Prieto D. AMPK, metabolism, and vascular function. *The FEBS Journal*. 2021;288:3746–3771.
21. Dengler F. Activation of AMPK under Hypoxia: Many Roads Leading to Rome. *IJMS*. 2020;21:2428.
22. Cantó C, Gerhart-Hines Z, Feige JN, Lagouge M, Noriega L, Milne JC, Elliott PJ, Puigserver P, Auwerx J. AMPK regulates energy expenditure by modulating NAD+ metabolism and SIRT1 activity. *Nature*. 2009;458:1056–1060.
23. Lan F, Cacicedo JM, Ruderman N, Ido Y. SIRT1 Modulation of the Acetylation Status, Cytosolic Localization, and Activity of LKB1. *Journal of Biological Chemistry*. 2008;283:27628–27635.
24. Cooke JP, Meng S. Vascular Regeneration in Peripheral Artery Disease. *ATVB*. 2020;40:1627–1634.
25. Wahlberg E. Angiogenesis and arteriogenesis in limb ischemia. *Journal of Vascular Surgery*. 2003;38:198–203.
26. Han J, Luo L, Marcelina O, Kasim V, Wu S. Therapeutic angiogenesis-based strategy for peripheral artery disease. *Theranostics*. 2022;12:5015–5033.
27. Yang J, Ii M, Kamei N, Alev C, Kwon S-M, Kawamoto A, Akimaru H, Masuda H, Sawa Y, Asahara T. CD34+ Cells Represent Highly Functional Endothelial Progenitor Cells in Murine Bone Marrow. *PLoS ONE*. 2011;6:e20219.
28. Van Huyen J-PD, Smadja DM, Bruneval P, Gaussem P, Dal-Cortivo L, Julia P, Fiessinger J-N, Cavazzana-Calvo M, Aiach M, Emmerich J. Bone marrow-derived mononuclear cell therapy induces distal angiogenesis after local injection in critical leg ischemia. *Modern Pathology*. 2008;21:837–846.
29. Dong Z, Pan T, Fang Y, Wei Z, Gu S, Fang G, Liu Y, Luo Y, Liu H, Zhang T, et al. Purified CD34+ cells versus peripheral blood mononuclear cells in the treatment of angiitis-induced no-option critical limb ischaemia: 12-Month results of a prospective randomised single-blinded non-inferiority trial. *EBioMedicine*. 2018;35:46–57.
30. Calvier L, Miana M, Reboul P, Cachofeiro V, Martinez-Martinez E, De Boer RA, Poirier F, Lacolley P, Zannad F, Rossignol P, et al. Galectin-3 Mediates Aldosterone-Induced Vascular Fibrosis. *ATVB*. 2013;33:67–75.
31. Ding N, Yang C, Ballew SH, Kalbaugh CA, McEvoy JW, Salameh M, Aguilar D, Hoogeveen RC, Nambi V, Selvin E, et al. Fibrosis and Inflammatory Markers and

549 Long-Term Risk of Peripheral Artery Disease: The ARIC Study. *ATVB*.
550 2020;40:2322–2331.
551 32. Bhattacharyya S, Wang W, Morales-Nebreda L, Feng G, Wu M, Zhou X, Lafyatis
552 R, Lee J, Hinchcliff M, Feghali-Bostwick C, et al. Tenascin-C drives persistence of
553 organ fibrosis. *Nat Commun*. 2016;7:11703.
554 33. Eppig JT. Mouse Genome Informatics (MGI) Resource: Genetic, Genomic, and
555 Biological Knowledgebase for the Laboratory Mouse. *ILAR Journal*. 2017;58:17–
556 41.
557 34. Wang Y, Roche O, Xu C, Moriyama EH, Heir P, Chung J, Roos FC, Chen Y, Finak
558 G, Milosevic M, et al. Hypoxia promotes ligand-independent EGF receptor signaling
559 via hypoxia-inducible factor–mediated upregulation of caveolin-1. *Proc. Natl. Acad.*
560 *Sci. U.S.A.* 2012;109:4892–4897.
561 35. Sonveaux P, Martinive P, DeWever J, Batova Z, Daneau G, Pelat M, Ghisdal P,
562 Grégoire V, Dessy C, Balligand J-L, et al. Caveolin-1 Expression Is Critical for
563 Vascular Endothelial Growth Factor–Induced Ischemic Hindlimb Collateralization
564 and Nitric Oxide–Mediated Angiogenesis. *Circulation Research*. 2004;95:154–161.
565 36. Bagali S, Das KK. Hypoxia and its preconditioning on cardiac and vascular
566 remodelling in experimental animals. *Respiratory Physiology & Neurobiology*.
567 2021;285:103588.
568 37. Joharapurkar AA, Pandya VB, Patel VJ, Desai RC, Jain MR. Prolyl Hydroxylase
569 Inhibitors: A Breakthrough in the Therapy of Anemia Associated with Chronic
570 Diseases. *J. Med. Chem.* 2018;61:6964–6982.
571 38. Prados ME, Correa-Sáez A, Unciti-Broceta JD, Garrido-Rodríguez M, Jimenez-
572 Jimenez C, Mazzone M, Minassi A, Appendino G, Calzado MA, Muñoz E. Betulinic
573 Acid Hydroxamate is Neuroprotective and Induces Protein Phosphatase 2A-
574 Dependent HIF-1α Stabilization and Post-transcriptional Dephosphorylation of
575 Prolyl Hydrolase 2. *Neurotherapeutics*. 2021;18:1849–1861.
576 39. Rahtu-Korpela L, Määttä J, Dimova EY, Hörkkö S, Gylling H, Walkinshaw G,
577 Hakkola J, Kivirikko KI, Myllyharju J, Serpi R, et al. Hypoxia-Inducible Factor
578 Prolyl 4-Hydroxylase-2 Inhibition Protects Against Development of Atherosclerosis.
579 *ATVB*. 2016;36:608–617.
580 40. Kumar D, Branch BG, Pattillo CB, Hood J, Thoma S, Simpson S, Illum S, Arora N,
581 Chidlow JH, Langston W, et al. Chronic sodium nitrite therapy augments ischemia-
582 induced angiogenesis and arteriogenesis. *Proc. Natl. Acad. Sci. U.S.A.*
583 2008;105:7540–7545.
584 41. Takahashi N, Shibata R, Ouchi N, Sugimoto M, Murohara T, Komori K. Metformin
585 stimulates ischemia-induced revascularization through an eNOS dependent pathway
586 in the ischemic hindlimb mice model. *Journal of Vascular Surgery*. 2015;61:489–
587 496.
588 42. Chen S, Yin C, Lao T, Liang D, He D, Wang C, Sang N. AMPK-HDAC5 pathway
589 facilitates nuclear accumulation of HIF-1α and functional activation of HIF-1 by
590 deacetylating Hsp70 in the cytosol. *Cell Cycle*. 2015;14:2520–2536.
591 43. Laemmle A, Lechleiter A, Roh V, Schwarz C, Portmann S, Furer C, Keogh A,
592 Tschan MP, Candinas D, Vorburger SA, et al. Inhibition of SIRT1 Impairs the
593 Accumulation and Transcriptional Activity of HIF-1α Protein under Hypoxic
594 Conditions. *PLoS ONE*. 2012;7:e33433.
595 44. Prados ME, Navarrete C, García-Martín A, Lastres-Cubillo I, Ponce-Díaz F,
596 Martínez-Orgado J, Muñoz E. VCE-005.1, an hypoxia mimetic betulinic acid
597 derivative, induces angiogenesis and shows efficacy in a murine model of traumatic
598 brain injury. *Biomedicine & Pharmacotherapy*. 2023;162:114715.

45. Yang X, Shang D. The role of peroxisome proliferator-activated receptor γ in lipid metabolism and inflammation in atherosclerosis. *Cell Biology International*. 2023;47:1469–1487.
46. Xu X, Guo H, Jing Z, Yang L, Chen C, Peng L, Wang X, Yan L, Ye R, Jin X, et al. N-Oleoylethanolamine Reduces Inflammatory Cytokines and Adhesion Molecules in TNF-α-induced Human Umbilical Vein Endothelial Cells by Activating CB2 and PPAR-α. *Journal of Cardiovascular Pharmacology*. 2016;68:280–291.
47. Steffens S, Pacher P. Targeting cannabinoid receptor CB_2 in cardiovascular disorders: promises and controversies. *British J Pharmacology*. 2012;167:313–323.
48. Li AC, Binder CJ, Gutierrez A, Brown KK, Plotkin CR, Pattison JW, Valledor AF, Davis RA, Willson TM, Witztum JL, et al. Differential inhibition of macrophage foam-cell formation and atherosclerosis in mice by PPARα, β/δ, and γ. *J. Clin. Invest.* 2004;114:1564–1576.
49. Turcotte C, Blanchet M-R, Laviolette M, Flamand N. The CB2 receptor and its role as a regulator of inflammation. *Cell. Mol. Life Sci.* 2016;73:4449–4470.
50. Ryszkiewicz P, Malinowska B, Schlicker E. Polypharmacology: promises and new drugs in 2022. *Pharmacol. Rep*. 2023;75:755–770.

619 **FIGURE LEGENDS**

620

621 **Figure 1**. **VCE-004.8 induces B55α/PP2A expression and activates HIF-1α in**
622 **endothelial EA.hy926 cells. A,** Representative images of B55α expression in EA.hy926
623 cells untreated and treated with VCE-004.8 for 24 h. Magnified region (marked by the
624 white rectangle) shows preferential perinuclear expression of B55α as indicated by white
625 arrows. **B,** EA.hy926 cells were transfected with siB55α or scrambled siRNAs (siCTR)
626 and 48 h later treated with VCE-004.8 for 3 h. B55α and HIF-1α protein expression was
627 analyzed by immunoblotting. **C,** Effect of VCE-004.8 on cell viability. EA.hy926 cells
628 were pre-incubated with increasing concentrations of VCE-004.8 during 1 h and then
629 were exposed to H_2O_2 for 24 h. Cell viability was calculated by MTT assay. The data
630 passed the normality test performed by the Kolmogorov-Smirnov test. P value is
631 calculated using 1-way ANOVA followed by Tukey post hoc multiple comparisons to
632 compare between the groups (n>4 independent experiments per group), the results are
633 shown as mean ± SEM. **D**, The cytoprotection mediated by VCE-004.8 is partially
634 dependent on HIF-1α activation. EA.hy926 cells were pretreated with VCE-004.8 in the
635 absence and the presence of the HIF-1α inhibitor YC-1 and then exposed to H_2O_2. Cell
636 viability was calculated by MTT assay. The data passed the normality test performed by
637 the Shaphiro-Wilk test. P value is calculated using 1-way ANOVA followed by Tukey
638 post hoc multiple comparisons to compare between the groups (n>3 independent
639 experiments per group); the results are shown as means ± SEM. P values indicated in
640 panels, significant as **p<0.01, ***p<0.001 ****p<0.0001.

641

642 **Figure 2**. **VCE-004.8 activates AMPK/Sirt1 pathway and prevents cellular**
643 **senescence**. **A,** HEK-293T cells preincubated with or without DS for 30 min and
644 stimulated for 3 h with increasing concentrations of VCE-004.8 and the steady state levels
645 of pAMPK total AMPK and actin detected by western blot. **B,** EA.hy296 cells were
646 stimulated with VCE-004.8 for 3h and the expression of Sirt1 and Visfatin (NAMPT) was
647 analyzed by western blot. **C,** VCE-004.8 induces Sirt1 activity measured by a
648 fluorometric assay. SRT1720 was used as a positive control. Data represent the mean ±
649 SD (n = 3). **D,** NAD^+/NADH ratio was determined in EA.hy296 cells with a NAD^+
650 /NADH assay kit. The data passed the normality test performed by the Shaphiro-Wilk
651 test. P value is calculated using 1-way ANOVA followed by Tukey post hoc multiple

652 comparisons to compare between the groups (n=3 independent experiments per group);
653 the results are shown as means ± SEM. P value indicated in panel, significant as **p<0.01.
654 **E,** VCE-004.8 prevents H_2O_2-induced senescence measured by SA-β-gal staining in
655 HMEC-1 cells. The data passed the normality test performed by the D'Agostino &
656 Pearson test. P value is calculated using 1-way ANOVA followed by Tukey post hoc
657 multiple comparisons to compare between the groups (n>18 represent areas of cell surface
658 from 3 independent experiments), the results are shown as means ± SD. P values indicated
659 in panel, significant as ****p<0.0001. **F,** HMEC-1 cells were incubated with VCE-004.8
660 and exposed to H_2O_2 and the expression of Sirt1, p21 and tubulin detected by western
661 blot.
662
663 **Figure 3**. **VCE-004.8 induces eNOS activation and NO synthesis in a B55α**
664 **dependent manner.** **A**. EA.hy926 cells were treated with VCE-004.8 for 3 h
665 Representative western blot of three independent experiments is shown. **B,** VCE-004.8
666 induces NO production. EA.hy296 cells were seeded, preincubated with DAF-2DA and
667 treated with sulforaphane (50 μM) or VCE-004.8 (10μM). The figure indicated the
668 percentage NO induction. The data passed the normality test performed by the Shaphiro-
669 Wilk test. P value is calculated using 1-way ANOVA followed by Tukey post hoc
670 multiple comparisons to compare between the groups (n=3 independent experiments per
671 group); the results are shown as means ± SD. P value indicated in panel, significant as
672 ****p<0.0001. **C,** VCE-004.8 induces eNOS phosphorylation in vascular endothelial
673 cells in a B55α dependent manner. EA.hy296 cells were transfected with siB55α or
674 scrambled siRNAs (siCTR) and 48 h later treated with VCE-004.8 for 3 h. Representative
675 western blot of three independent experiments is shown.
676
677 **Figure 4**. **Effects of oral VCE-004.8 in a Critical Limb Ischemia mouse model**. **A,**
678 Representative whole-mount images of Microfil vascular cast limbs 10 days after
679 ischemia, Micro-CT reconstruction and their segmentation of arterial vasculature 28 days
680 after femoral artery ligation. Collateral artery growth is indicated by black arrows. **B,**
681 Expression of *Vegf-a*, *Epo*, *Hgf*, and *Hif1α* mRNA in the gastrocnemius after 10 days of
682 ischemia. The data passed the normality test performed by the Shaphiro-Wilk test. P value
683 is calculated using 1-way ANOVA followed by Tukey post hoc multiple comparisons to

684 compare between the groups (n=3 animals per group); the results are shown as means ±
685 SEM. P value indicated in panel, significant as *p < 0.05; **p < 0.01.
686
687 **Figure 5**. **Oral VCE-004.8 enhances ischemia-induced vessel formation and vascular**
688 **endothelial cells proliferation *in vivo*. A.** Double immunofluorescence confocal staining
689 of α-SMA (green)/CD31 (red) in gastrocnemius muscles 28 day after ischemia. The
690 immunofluorescence was used to quantify the number of vessel peer area and the
691 perimeter of the lumen vessel in mouse muscle. As the data cannot passed the normality
692 test. P values are calculated using a nonparametric Kruskal-Wallis test followed by Dunn
693 multiple. The results are shown as mean ± SEM. P values indicated in panels, significant
694 as **p < 0.01, ***p<0.001, ****p<0.0001. **B,** The number of $CD31^+/Ki67^+$ positive cells
695 per area and number of $CD31^+/Ki67^+$ cells per total cells were quantified using double
696 immunofluorescence confocal staining of CD31 (green) and Ki67 (red) in gastrocnemius
697 muscles 28 day after ischemia. Significance was determined by one-way ANOVA
698 followed by Tukey´s test. The results are shown as means ± SEM (n=3). P values
699 indicated in panels, significant as ****p < 0.0001.
700
701 **Figure 6**. **Oral VCE-004.8 enhanced ischemia-induced *de novo* vessel and alleviated**
702 **fibrosis *in vivo*. A,** Double immunofluorescence confocal staining of CD34
703 (green)/CD31 (red) in gastrocnemius muscles 28 days was used to calculate the number
704 of $CD34^+/CD31^-$ cells (immature endothelial vascular cells) and $CD34^+/CD31^+$ (mature
705 endothelial vascular cells). Values are mean ± SEM (n = 3-4). In both quantifications, the
706 significance was determined by one-way ANOVA non-parametric followed by a
707 Kruskal–Wallis test. P values indicated in panels, significant as **p < 0,01; ***p < 0.001;
708 ****p < 0.0001. **B,** Immunofluorescence staining of TNC (green) in gastrocnemius
709 muscles 28 days after ischemia and quantifications. Values are mean ± SEM (n = 3-4),
710 and significance was determined by one-way ANOVA non-parametric followed by
711 Kruskal–Wallis test. P values indicated in panels, significant as ***p < 0.001; ****p <
712 0.0001. **C,** Representative immunofluorescence staining of TNC in cross-section of
713 healthy and disease human arteries.
714
715 **Figure 7**. **Effects of VCE-004.8 on B55α and Sirt1 expression *in vivo*. A,**
716 Representative double immunofluorescence confocal staining of B55α (red)/CD31
717 (green) (left) and immunofluorescence staining of Sirt1(green) (right) in gastrocnemius

718 muscles 10 days after ischemia. **B,** Quantifications of B55α (left) and Sirt1 (right)
719 staining in gastrocnemius muscles 10 days after ischemia. For B55α and Sirt1
720 quantification, the data do not pass the normality test performed and the significance was
721 determined non-parametric followed by a Kruskal–Wallis test. Values are mean ± SEM
722 (n = 3-4). P values indicated in panels, significant as *p < 0.05 as **p < 0.01; ***p <
723 0.001. **C,** Expression of *B55α* and *Sirt1* mRNA in mice gastrocnemius at 10 days after
724 femoral ligation. The data passed the normality test performed by the Shaphiro-Wilk test.
725 P value is calculated using 1-way ANOVA followed by Tukey post hoc multiple
726 comparisons to compare between the groups (n=3 animals per group). The results are
727 shown as mean ± SEM. P value indicated in panel, significant as *p < 0.05; **p < 0.01;
728 ***p < 0.001; ****p < 0.0001. **D,** Representative immunofluorescence image of
729 B55α (red) in cross-section of healthy and disease human arteries (left) and representative
730 double immunofluorescence staining of Sirt1 (green) and CD31(red) in cross-section of
731 healthy and disease human arteries (right). Magnified region (white rectangle) showing
732 details of Sirt1 expression (yellow arrow).
733
734 **Figure 8**. **Oral VCE-004.8 induces CAV1 *in vivo*.** **A**, Overview of laser capture
735 microdissection. Representative images vessel marked with αSMA in gastrocnemius
736 before (left) and after (right) laser dissection indicated by red asterisk. **B**, Heatmap
737 showing the expression levels for the resulting list of 11 proteins. Color indicates the
738 mean of scaled regularized log transformed expression values. Red square indicates
739 CAV1. **C.** Representatives images of double immunostaining of CAV1(red) and CD31
740 (green) in gastrocnemius 10 days after ischemia (left) and the CAV1 staining
741 quantification (right). The significance was determined non-parametric followed by a
742 Kruskal–Wallis test. In both quantification, values are mean ± SEM, (n = 3). P values
743 indicated in panels, significant as *p < 0.05. **D,** The expression of *Cav1* mRNA in mice
744 gastrocnemius at 10 days. The data passed the normality test performed by the Shaphiro-
745 Wilk test. P value is calculated using 1-way ANOVA followed by Tukey post hoc
746 multiple comparisons to compare between the groups test (n=3 animals per group). The
747 results are shown as mean ± SEM. Values indicated in panels, significant as *p < 0.05;
748 **p < 0.01. **E,** Representative immunofluorescence staining of CAV1 in cross-section of
749 healthy and disease human arteries.
750

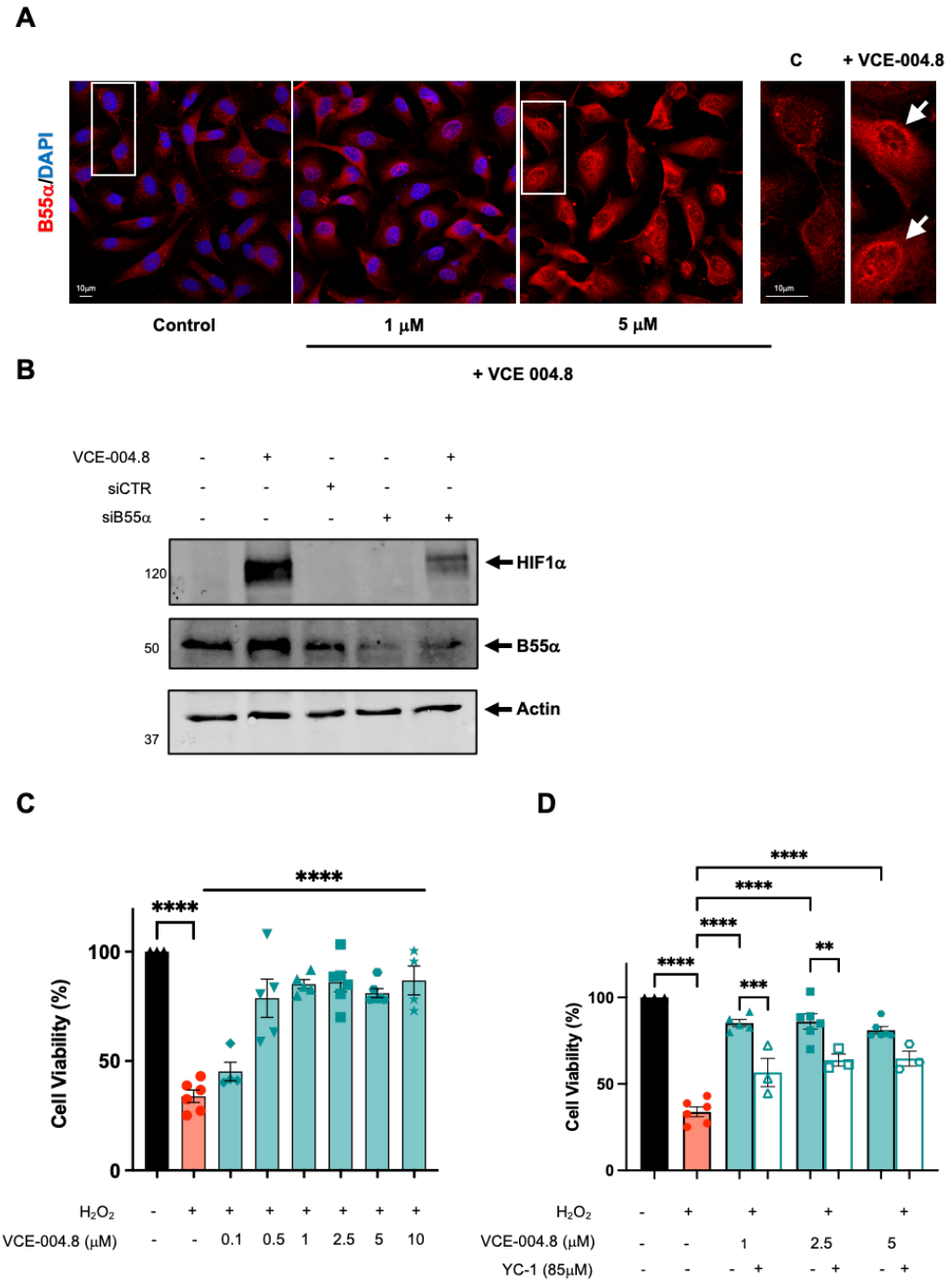
A
C
+ VCE-004.8
B55α/DAPI
Control
1 µM
5 µM
+ VCE 004.8
B
VCE-004.8
siCTR
siB55α
HIF1α
B55α
Actin
120
50
37
C
D
Cell Viability (%)
H2O2
VCE-004.8 (µM)
YC-1 (85µM)

Figure 1

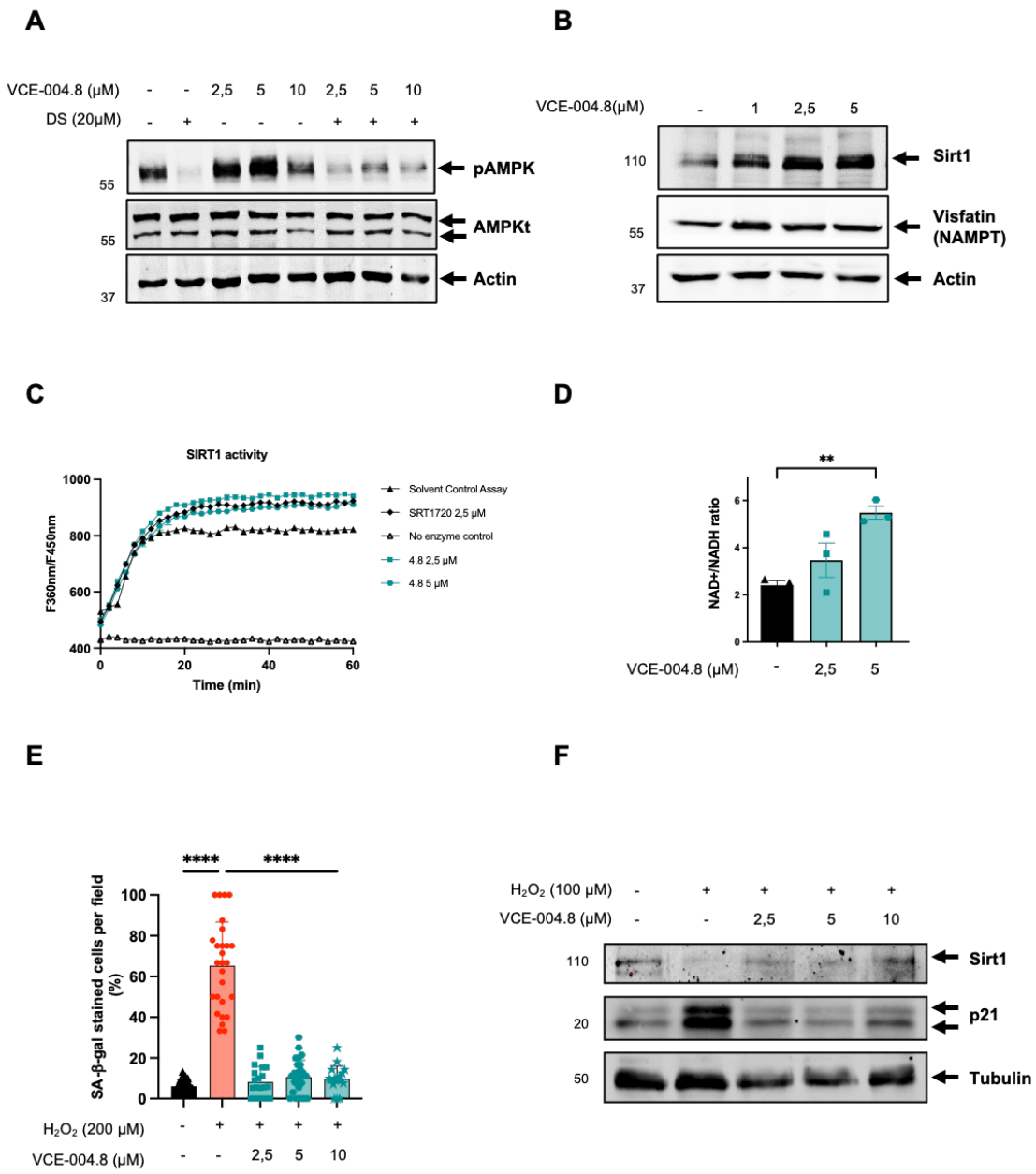
A
VCE-004.8 (μM) - - 2,5 5 10 2,5 5 10
DS (20μM) - + - - - + + +
55
55
37
pAMPK
AMPKt
Actin
B
VCE-004.8(μM) - 1 2,5 5
110
55
37
Sirt1
Visfatin (NAMPT)
Actin
C
SIRT1 activity
F360nm/F450nm
1000
800
600
400
0
20
40
60
Time (min)
Solvent Control Assay
SRT1720 2,5 μM
No enzyme control
4.8 2,5 μM
4.8 5 μM
D
**
NAD+/NADH ratio
6
4
2
0
VCE-004.8 (μM) - 2,5 5
E
****
****
SA-β-gal stained cells per field (%)
100
80
60
40
20
0
H2O2 (200 μM) - + + + +
VCE-004.8 (μM) - - 2,5 5 10
F
H2O2 (100 μM) - + + + +
VCE-004.8 (μM) - - 2,5 5 10
110
20
50
Sirt1
p21
Tubulin

Figure 2

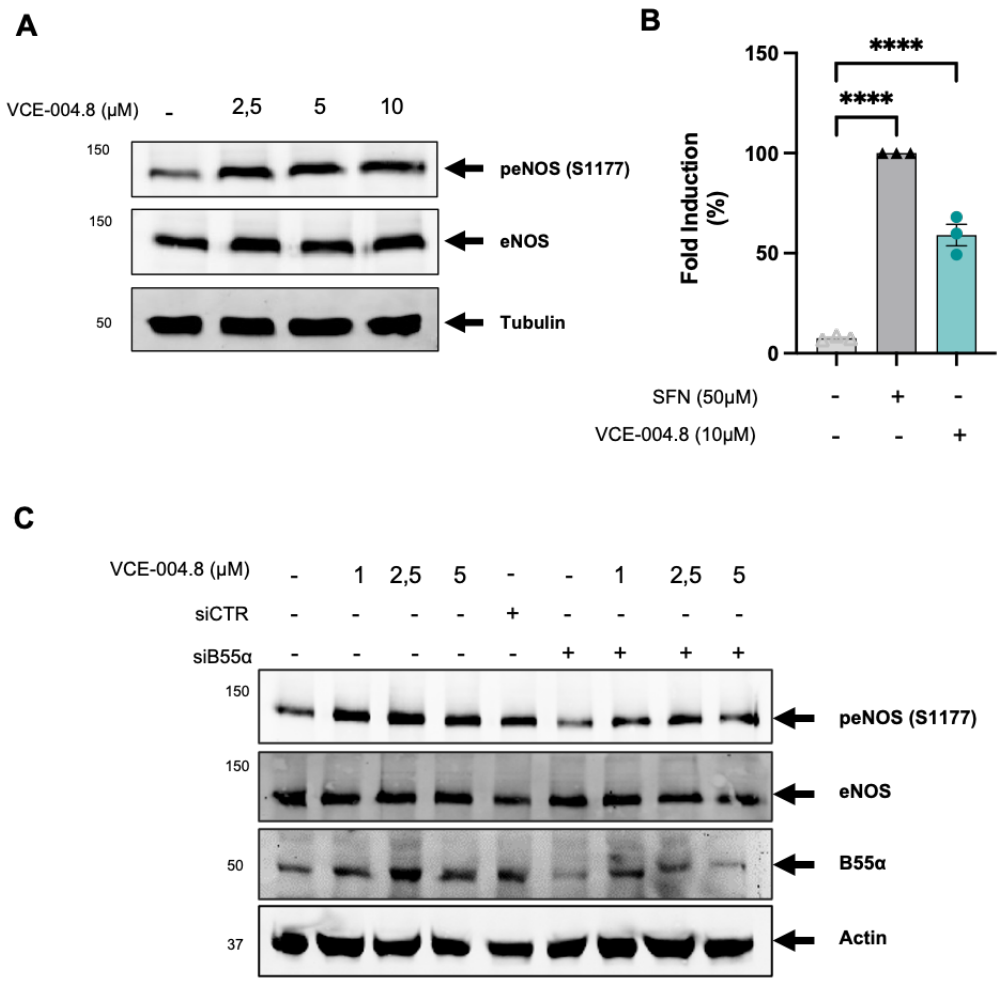
A
VCE-004.8 (μM)
-
2,5
5
10
150
150
50
peNOS (S1177)
eNOS
Tubulin
B
Fold Induction (%)
150
100
50
0
****
****
SFN (50μM)
VCE-004.8 (10μM)
C
VCE-004.8 (μM)
siCTR
siB55α
150
150
50
37
peNOS (S1177)
eNOS
B55α
Actin

Figure 3

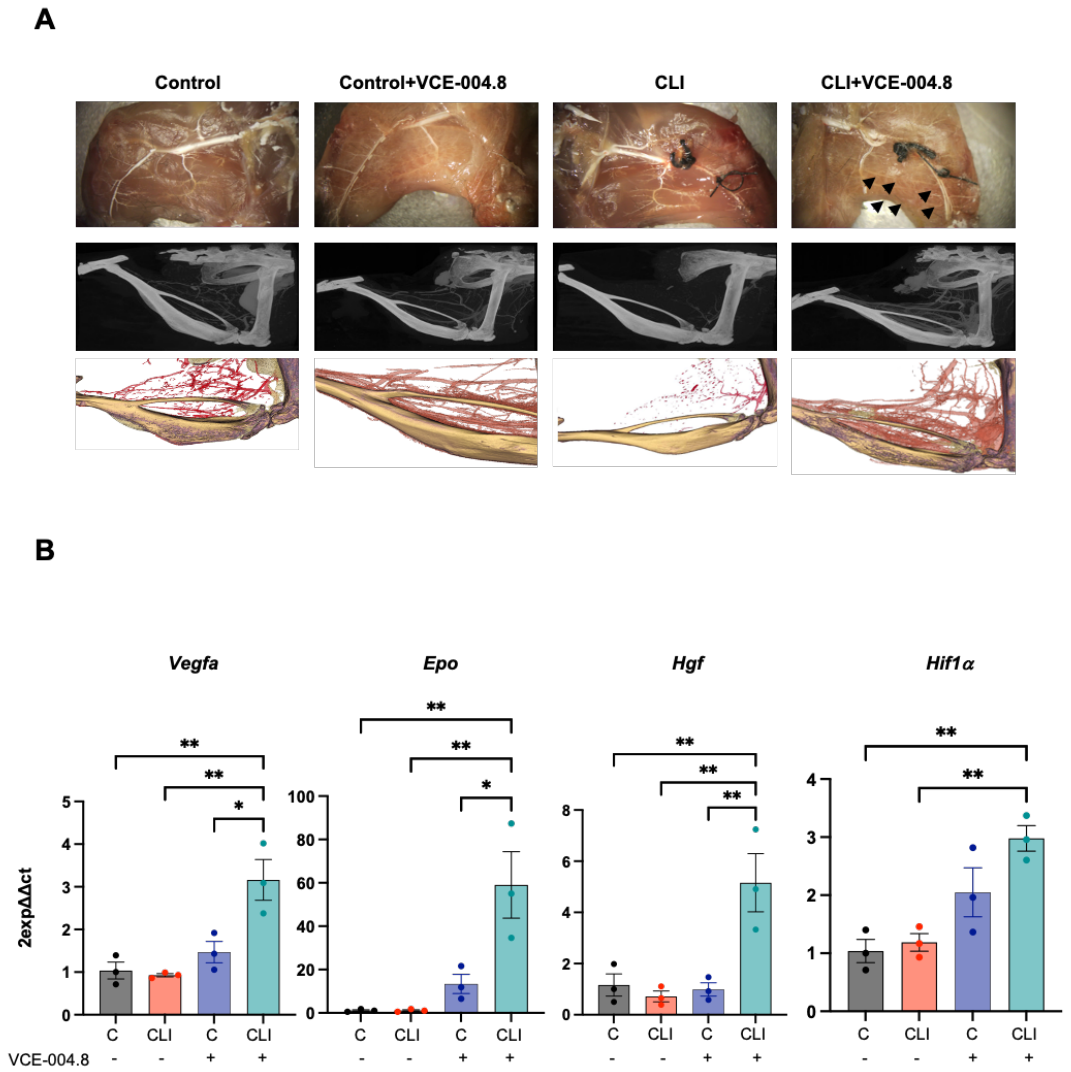
A
Control
Control+VCE-004.8
CLI
CLI+VCE-004.8
B
Vegfa
Epo
Hgf
Hif1α
2expΔΔct
C
CLI
C
CLI
VCE-004.8
-
-
+
+

Figure 4

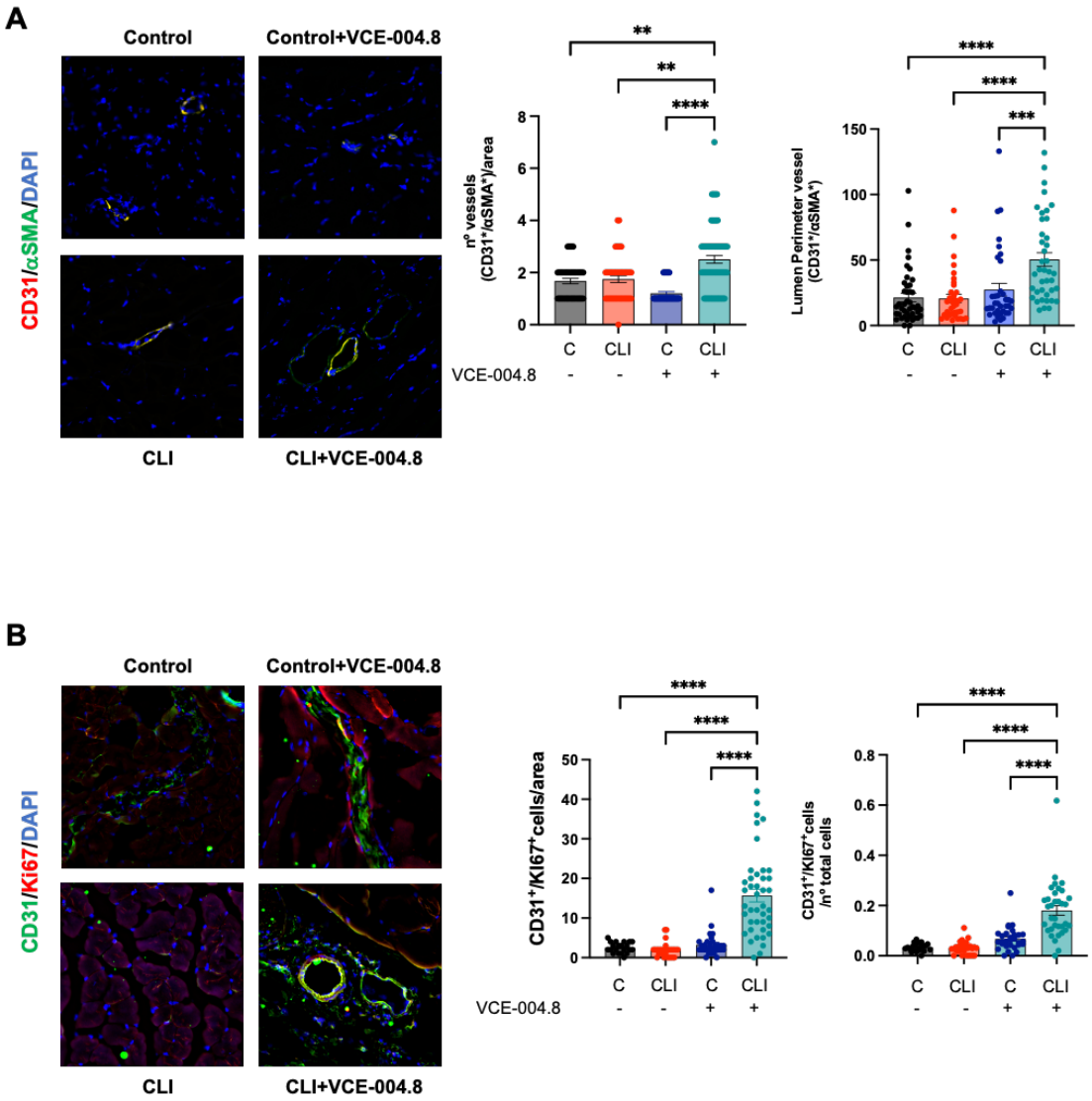
A
Control
Control+VCE-004.8
CD31/αSMA/DAPI
CLI
CLI+VCE-004.8
nº vessels (CD31⁺/αSMA⁺)/area
Lumen Perimeter vessel (CD31⁺/αSMA⁺)
C
CLI
VCE-004.8
B
CD31/Ki67/DAPI
CD31⁺/KI67⁺cells/area
CD31⁺/KI67⁺cells /nº total cells

Figure 5

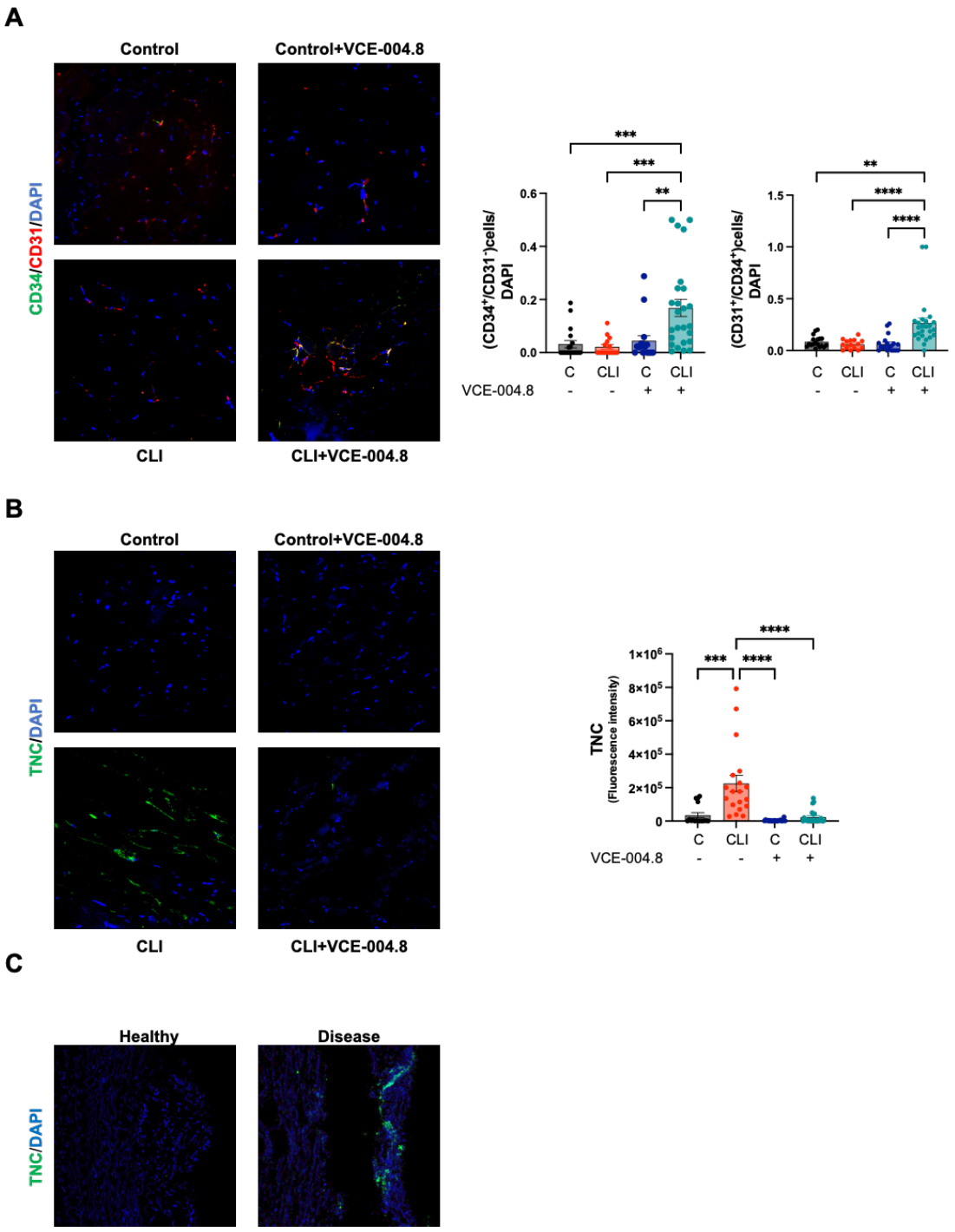
A
Control
Control+VCE-004.8
CD34/CD31/DAPI
CLI
CLI+VCE-004.8
(CD34+/CD31-)cells/ DAPI
(CD31+/CD34+)cells/ DAPI
C
CLI
VCE-004.8
B
TNC/DAPI
TNC (Fluorescence intensity)
C
Healthy
Disease

Figure 6

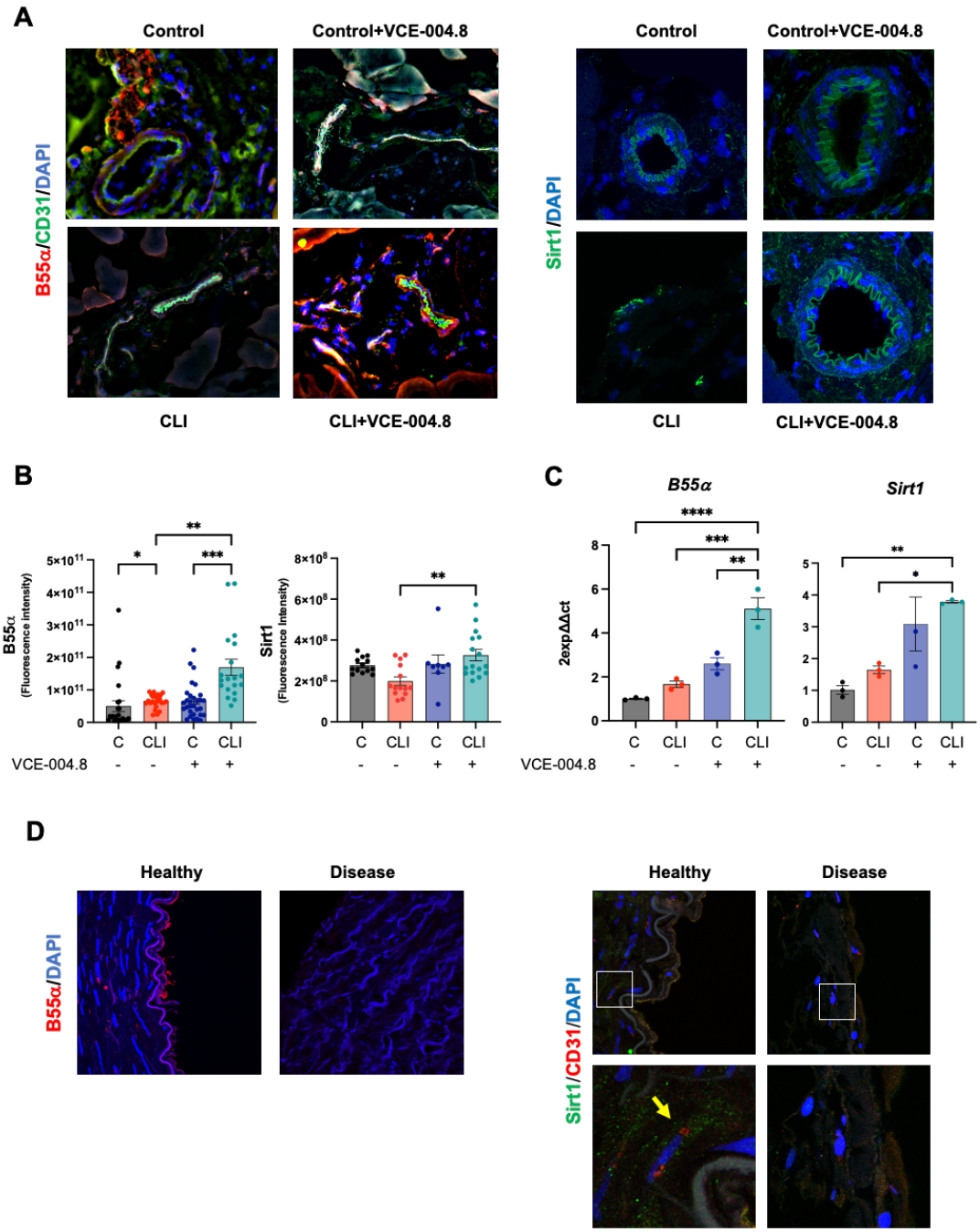
A
Control
Control+VCE-004.8
B55α/CD31/DAPI
CLI
CLI+VCE-004.8
Control
Control+VCE-004.8
Sirt1/DAPI
CLI
CLI+VCE-004.8
B
B55α
(Fluorescence intensity)
Sirt1
(Fluorescence Intensity)
C
C
CLI
VCE-004.8
B55α
Sirt1
2expΔΔct
D
Healthy
Disease
B55α/DAPI
Healthy
Disease
Sirt1/CD31/DAPI

Figure 7

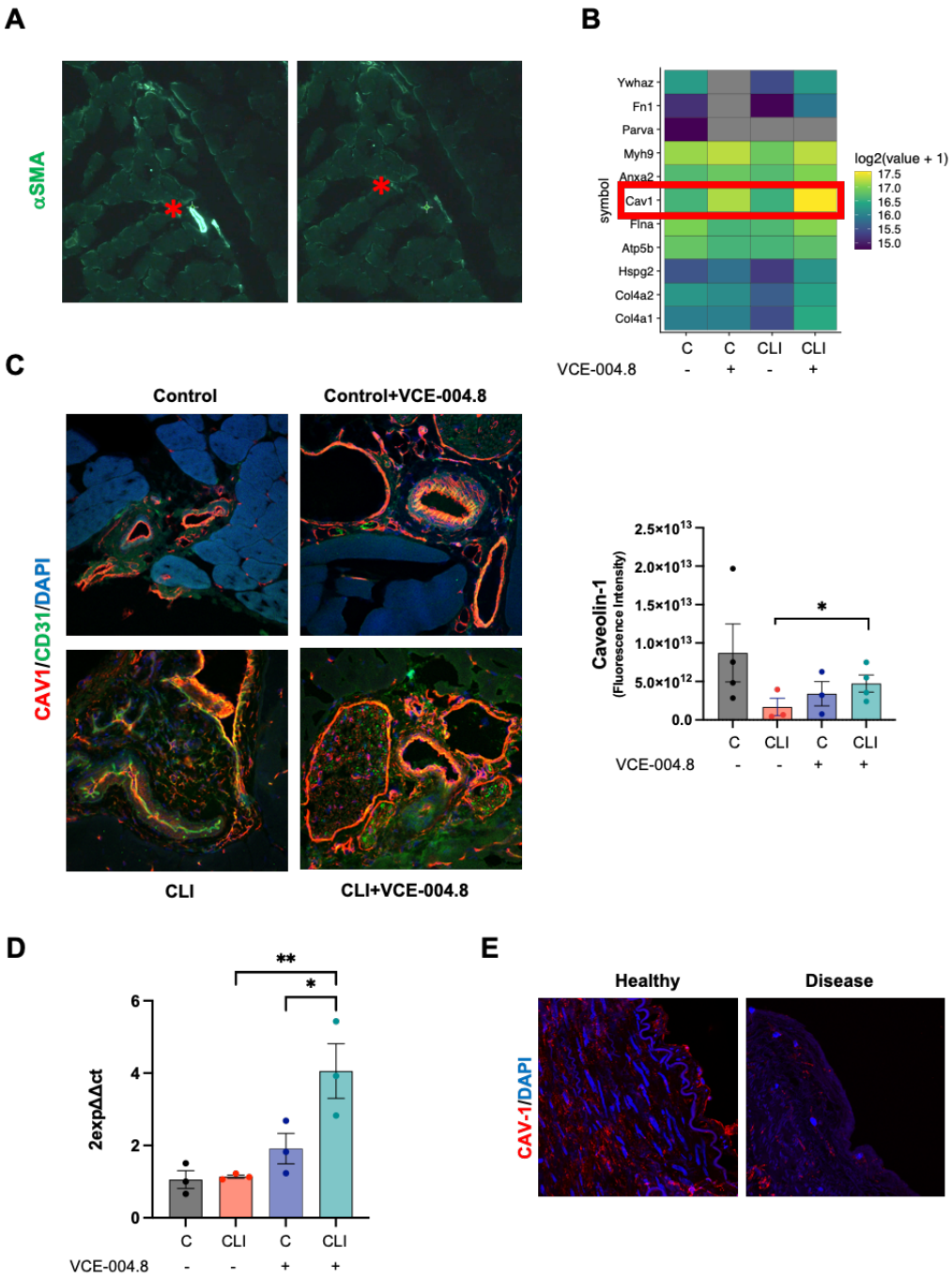
A
αSMA
B
Ywhaz
Fn1
Parva
Myh9
Anxa2
Cav1
Flna
Atp5b
Hspg2
Col4a2
Col4a1
symbol
log2(value + 1)
17.5
17.0
16.5
16.0
15.5
15.0
C C CLI CLI
VCE-004.8 - + - +
C
Control
Control+VCE-004.8
CAV1/CD31/DAPI
CLI
CLI+VCE-004.8
Caveolin-1
(Fluorescence Intensity)
2.5×10^13
2.0×10^13
1.5×10^13
1.0×10^13
5.0×10^12
0.0
*
C CLI C CLI
VCE-004.8 - - + +
D
**
*
2expΔΔct
6
4
2
0
C CLI C CLI
VCE-004.8 - - + +
E
Healthy
Disease
CAV-1/DAPI

Figure 8